

Mass Spectrometry and Machine Learning Reveal Determinants of Client Recognition by Antiamyloid Chaperones

Authors

Nicklas Österlund, Thibault Vosselman, Axel Leppert, Astrid Gräslund, Hans Jörnvall, Leopold L. Ilag, Erik G. Marklund, Arne Elofsson, Jan Johansson, Cagla Sahin, and Michael Landreh

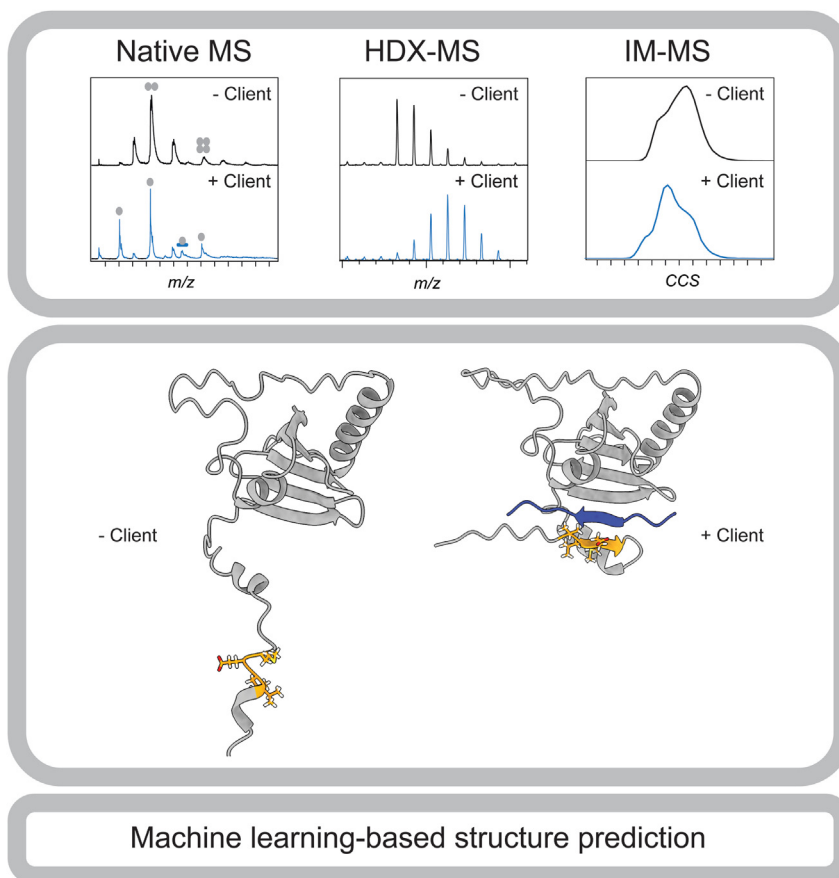
Correspondence

Cagla.Sahin@ki.se; Michael.Landreh@ki.se

In Brief

A wide range of proteins can prevent amyloid formation *in vitro* and *in vivo*, but the exact nature of these interactions is unclear. By combining machine learning-based structure prediction of protein complexes with mass spectrometry, we can discern the molecular determinants of specific and nonspecific chaperone-client interactions.










Graphical Abstract



Highlights

- Chaperone-client interactions are hard to capture in structural biology.
- Machine learning can generate possible chaperone complex structures.
- Mass spectrometry can identify complex architectures and interaction sites.
- The combination reveals how specific and nonspecific chaperone interactions differ.

Mass Spectrometry and Machine Learning Reveal Determinants of Client Recognition by Antiamyloid Chaperones

Nicklas Österlund¹, Thibault Vosselman^{2,†}, Axel Leppert^{2,†}, Astrid Gräslund¹, Hans Jörnvall³, Leopold L. Ilag⁴, Erik G. Marklund⁵, Arne Elofsson⁶, Jan Johansson⁷, Cagla Sahin^{2,8,*}, and Michael Landreh^{2,*}

The assembly of proteins and peptides into amyloid fibrils is causally linked to serious disorders such as Alzheimer's disease. Multiple proteins have been shown to prevent amyloid formation *in vitro* and *in vivo*, ranging from highly specific chaperone–client pairs to completely nonspecific binding of aggregation-prone peptides. The underlying interactions remain elusive. Here, we turn to the machine learning–based structure prediction algorithm AlphaFold2 to obtain models for the nonspecific interactions of β -lactoglobulin, transthyretin, or thioredoxin 80 with the model amyloid peptide amyloid β and the highly specific complex between the BRICHOS chaperone domain of C-terminal region of lung surfactant protein C and its polyvaline target. Using a combination of native mass spectrometry (MS) and ion mobility MS, we show that nonspecific chaperoning is driven predominantly by hydrophobic interactions of amyloid β with hydrophobic surfaces in β -lactoglobulin, transthyretin, and thioredoxin 80, and in part regulated by oligomer stability. For C-terminal region of lung surfactant protein C, native MS and hydrogen–deuterium exchange MS reveal that a disordered region recognizes the polyvaline target by forming a complementary β -strand. Hence, we show that AlphaFold2 and MS can yield atomistic models of hard-to-capture protein interactions that reveal different chaperoning mechanisms based on separate ligand properties and may provide possible clues for specific therapeutic intervention.

Fibrillar protein aggregates have been observed in a wide range of diseases, including cancer, systemic amyloidosis, and interstitial lung disease (1–3). They are, however, mostly associated with neurodegenerative disorders, such as Alzheimer's disease (AD) and Parkinson's disease (4). The

assembly of proteins or peptides into highly ordered β -sheet-rich amyloid fibrils can give rise to pathological conditions through the formation of toxic intermediates that cause cell damage, loss of function of the aggregating protein, and/or accumulation of fibrillar material (5, 6). Consequently, development of therapeutic strategies has often focused on preventing or reversing the aggregation process (7). Some clues for targeted intervention can be gathered from nature, as the ability to form fibrils is widespread in the proteome (8). Aggregation processes are however under normal cellular conditions tightly regulated to prevent detrimental effects. Several proteins have been found to have antiamyloid activity by blocking aggregation or stabilizing the native state of their client. Protein systems with antiamyloid activity are diverse, ranging from dedicated chaperones such as small heat shock proteins to proteins with unrelated physiological functions, like serum albumin (9–11). However, amyloid-forming proteins have a challenging chemical nature, often combining conformational flexibility and poor solubility. Therefore, detailed structural information that exactly reveals how proteins counteract fibril formation has remained scarce.

We have previously reported antiamyloid activity in proteins whose biological contexts suggest significant differences in client specificity. For example, we have shown that the bovine whey protein β -lactoglobulin (β LG), along with several other analytical protein standards, such as bovine serum albumin, lysozyme, and pyruvate kinase, can prevent aggregation of the model amyloid β ($A\beta$) peptide *in vitro* (10). NMR spectroscopy analysis revealed that monomeric $A\beta$ broadly interacts with these proteins *via* hydrophobic interactions. The chaperone effect thus arises from indiscriminate contact and is most pronounced at or above near-stoichiometric ratios

From the ¹Department of Biochemistry and Biophysics, Stockholm University, Stockholm, Sweden; ²Department of Microbiology, Tumor and Cell Biology, and ³Department of Medical Biochemistry and Biophysics, Karolinska Institutet, Stockholm, Sweden; ⁴Department of Materials and Environmental Chemistry, Stockholm University, Stockholm, Sweden; ⁵Department of Chemistry - BMC, Uppsala University, Uppsala, Sweden; ⁶Science for Life Laboratory and Department of Biochemistry and Biophysics, Stockholm University, Solna, Sweden; ⁷Department of Biosciences and Nutrition, Karolinska Institutet, Neo, Huddinge, Sweden; ⁸Department of Biology, University of Copenhagen, Denmark

[†]These authors contributed equally to this work.

*For correspondence: Michael Landreh, Michael.Landreh@ki.se; Cagla Sahin, Cagla.Sahin@ki.se.

between chaperone and client. Several nonchaperone proteins with anti-amyloid activity have been implicated in protein aggregation diseases like AD. A prominent example is transthyretin (TTR), a transport protein that is itself related to amyloid disease upon destabilization of its native tetrameric state. TTR is known to inhibit *in vitro* aggregation of other amyloidogenic species including A β (12, 13), even though the exact interaction mode is disputed (14–16). Another example is T80, a thioredoxin variant that can prevent A β aggregation *in vitro*, and the levels of which are decreased in the cerebral spinal fluid of AD patients (17). T80 is produced by α -secretase cleavage of the C-terminal α -helix of thioredoxin, exposing a hydrophobic patch that has been linked to its anti-amyloid activity (17).

While β LG, TTR, and T80 are examples of nonspecific anti-amyloid chaperones, the proform of lung surfactant protein C (proSP-C) is the exact opposite. SP-C, a highly aggregation-prone transmembrane peptide located in the lipid bilayers of the alveolae, is synthesized with a C-terminal BRICHOS domain, homologs of which have been identified in several proteins associated with neurodegeneration and cancer (18). ProSP-C BRICHOS binds to the polyvaline region of SP-C, preventing its assembly into fibrils (19, 20). Mutations in the C-terminal region of proSP-C (CTC), composed of BRICHOS and a disordered region, give rise to SP-C amyloid deposits and lead to interstitial lung disease (21). X-ray crystallography revealed that proSP-C BRICHOS, containing a central β -sheet flanked by two helices, assembles into trimers (21). SP-C with its BRICHOS domain thus represents an example of a highly specific partner in a chaperone–client pair (22). The proSP-C BRICHOS domain is however also known to inhibit fibrilization of other amyloid-forming peptides, such as the A β peptide, indicating that the chaperone is capable of recognizing common amyloidogenic motifs (22). Although the differences in chaperone specificity between β LG and CTC are obvious from their biological contexts, no detailed models have been available that could reveal the structural determinants of their specificity, as data from NMR and X-ray crystallography have proven insufficient to solve the structures of both complexes.

Recently, the arrival of machine learning–driven protein structure prediction algorithms such as AlphaFold2 (AF2) and RosettaFold has enabled modeling of previously inaccessible protein complexes with an accuracy that rivals experimentally determined structures (23, 24). Thus, AF2 has also been found to reliably dock short peptides into binding pockets of folded protein domains (25). However, predictions are based on user input and will suggest the most likely structure of any protein–peptide pair provided. It can deliver seemingly plausible models for protein interactions not occurring under native conditions, and the resulting models require therefore further experimental validation. Mass spectrometry (MS) offers several good analytical strategies complementary to AF2 (26, 27):

1. The use of physiological buffer conditions and carefully tuned instrument parameters have enabled us to preserve noncovalent interactions during MS analysis. The mass of intact complexes thus reveals protein and ligand interactions. The approach commonly termed “native MS” can be employed to determine binding stoichiometries and relative complex stabilities.
2. In ion mobility (IM) measurements, protein ions are separated according to their collision cross-sections (CCSs) in a gas-filled cell, which provides information about the spatial arrangement of their components. This method can reveal conformational changes and topologies upon ligand binding in protein complexes.
3. Labeling in solution, when hydrogens in the protein backbone are exchanged for deuterium (HDX), can be paired with MS to reveal the spatial distribution of the labels. HDX-MS thus gives information about conformational dynamics of interaction sites.

Here, we have used a combination of AF2 (with its models of protein complexes) and structural MS (with its information on stoichiometries, topologies, and interaction sites) to unravel differences in anti-amyloid mechanisms. Using β LG, TTR, and A β , as well as CTC and polyvaline, we show how client β -strand propensity and hydrophobicity drive nonspecific and specific chaperone interactions, respectively.

EXPERIMENTAL PROCEDURES

Protein Preparations

β LG was purchased from Sigma, and wildtype recombinant A β (1–40) as a lyophilized powder was purchased from Alexo-Tech AB. Scrambled recombinant A β , with the sequence KVKGLIDGA-HIGDLVYEFMDSNSFR EGVGAGHVHVAQVEF, was purchased from rPeptide as a lyophilized powder. The peptides were dissolved in 6 M guanidine hydrochloride, purified by size-exclusion chromatography on a Superdex 75 Increase 10/300 GL column in 200 mM ammonium acetate (pH 6.9) to remove aggregated material, and stored on ice until analysis. Recombinant human T80 was purchased from R&D Systems, and recombinant human TTR from Alexo-Tech AB. CTC was prepared as described previously (21). Amidated and acetylated KKVVVVVVVKK (V7) and KKAAAAAAAKK (A7) were purchased from Thermo Electron.

Native MS

Native IM-MS of β LG and TTR was performed using a Waters Synapt G2S traveling-wave IM mass spectrometer, and native MS of T80 was performed on a Waters Synapt G1 traveling-wave IM mass spectrometer. Samples were ionized using offline borosilicate emitters (Thermo). The capillary voltage was 1.2 to 1.5 kV, and the cone voltage was 20 V. The source temperature was 25 °C, and the source pressure was 3.4 mbar. Wave height and wave velocity were 35 V and 700 m/s in the IM spectrometry cell and 10 V and 248 m/s in the transfer cell. The IM spectrometry gas was nitrogen with a flow of 50 ml/min, and the trap gas was argon with a flow of 10 ml/min. Mass spectra were processed using MassLynx 4.1 (Waters). IM-MS data were analyzed using PULSAR (version 2.0, 2018) (28). Drift tube CCS values for β LG and TTR were used to calibrate T-wave data. Theoretical CCS values were computed using projection approximation in IMPACT (29) and

scaled with the empirical factor of 1.14 (30). Native MS of CTC was performed on a Q-ToF Ultima API mass spectrometer (Waters) equipped with a Z-spray source using offline borosilicate emitters (Thermo). The source temperature was 30 °C, the capillary voltage was 1.5 kV, and the cone voltage was 20 V, respectively. The source pressure was maintained at 7 mbar. The mass spectrometer was operated in single-reflector mode.

HDX-MS

For HDX-MS of CTC, a CTC stock solution with a concentration of 0.9 mM (determined by absorption at 280 nm) was diluted in deuterated Tris buffer to a final deuterium content of 92.5% and protein concentration of 30 μ M. For peptide interaction studies, V7 or A7 was preincubated with CTC for 10 min at 22 °C at a molar ratio of 1:1 prior to deuteration. Aliquots of 20 μ l were collected from separate incubations after 1, 5, 10, 30, and 60 min. Fully deuterated protein was prepared by freeze-drying of a CTC aliquot followed by resuspension in 99.9% deuterium oxide and incubation for 4 h at 50 °C. Deuterium exchange was quenched by transfer of aliquots to chilled Eppendorf tubes containing 0.5 μ l of 5% TFA (Merck), subsequent vortexing, and freezing in liquid nitrogen until analysis. For MS analysis, deuterated aliquots were thawed and injected into an HPLC system submerged in an ice bath. Proteins were digested online in a Porozyme Immobilized Pepsin Cartridge (Applied Biosystems) operated at 17 μ l/min in 0.05% TFA. The peptides obtained were desalted for 10 min using a Waters Symmetry C18 trap column and eluted in a single step with 70% acetonitrile in 0.1% formic acid at a flow rate of 17 μ l/min. Samples were delivered to the mass spectrometer through a 50 μ m tapered tip emitter (New Objective), and spectra were acquired on a Waters Ultima API mass spectrometer (Waters) equipped with a Z-spray source at a source temperature of 80 °C, a capillary voltage of 1.7 kV, and cone and RF lens 1 potentials of 100 and 38 V, respectively. The mass scale was calibrated using [Glu1]-fibrinopeptide B. Scans were acquired for 5 min at a rate of one scan per 2 s between 300 and 2000 *m/z*.

AlphaFold2 Predictions

AF2 predictions were generated using ColabFold (<https://colab.research.google.com/github/sokrypton/ColabFold/blob/main/AlphaFold2.ipynb>), version 1.4, with default settings (five models, no AMBER step). Structures were visualized with ChimeraX, version 1.3 (<https://www.cgl.ucsf.edu/chimerax>).

Experimental Design and Statistical Rationale

Native MS and IM-MS experiments were repeated between two and four times, and no significant deviations were observed when identical instrument parameters were used. HDX-MS datasets were recorded in triplicates (three separate deuterium incubations). Deuteration was calculated as the average and standard deviation of the *m/z* values of the isotope envelope centroids on experimental triplicates using the Waters MassLynx software package. Data were plotted using the Prism software (GraphPad Software, Inc) as average *m/z* and standard deviation from three independent repeats. Deuteration curves were fitted for one-phase association (with near-maximum deuteration reached at the first time point) or two-phase association (with an observable time-dependent increase).

RESULTS AND DISCUSSION

The Nonchaperone Protein β LG Inhibits $A\beta$ Aggregation Via Binding to Hydrophobic Surfaces

The ability of β LG to prevent $A\beta$ aggregation has previously been attributed to nonspecific interactions that involve all

residues of the $A\beta$ peptide (10). To now obtain a more detailed insight into this association, we predicted the structure of β LG monomers and dimers in the presence and absence of $A\beta$ (Fig. 1A). The AF2 model of dimeric β LG is in near-perfect agreement with the crystal structure giving an RMSD of 0.674 Å excluding the disordered N-terminal region. We then predicted the structures of monomeric and dimeric β LG with $A\beta$. Overlaying the five AF2 models of the 1:1 β LG- $A\beta$ heterocomplex suggest $A\beta$ binding mostly to the β LG dimer interface of β LG and to a lesser extent to other hydrophobic regions of the protein (Fig. 1A). Similarly, the predicted complex of dimeric β LG with monomeric $A\beta$ did not indicate a preferred location for the peptide but rather a random placement with high positional alignment error scores, in line with the nonspecific association (Figs. 1B and S1). A surprising observation was that $A\beta$ appeared to distort the prediction of the dimer in some cases, although these models have high positional alignment error scores even for the dimer interface (supplemental Fig. S1). To test these models, we turned to native MS. Mass spectra recorded in the presence of $A\beta$ at physiological pH showed a decrease in the intensity of the β LG dimer peaks. We detected peaks corresponding in mass to a complex of $A\beta$ with dimeric as well as with monomeric β LG, which were further confirmed by MS/MS (Figs. 1C and S1). $A\beta$ with a scrambled sequence ($A\beta_{Scr}$) gave the same binding pattern as wildtype $A\beta$ (Fig. 1C). This observation supports the idea that the interaction is not sequence specific, as $A\beta$ and $A\beta_{Scr}$ have the exact same average hydrophobicity but different sequences. AF2 indeed suggests very similar interactions between $A\beta_{Scr}$ and β LG to what was observed with the native $A\beta$ peptide (supplemental Fig. S2). Binding does in both cases involve the most hydrophobic segments of the peptides, with $A\beta_{Scr}$ having a more even distribution of hydrophobicity compared with $A\beta$ (supplemental Fig. S2).

As the next step, we used IM-MS to determine the CCSs of the β LG- $A\beta$ complexes and compared them with the data from the AF2 predictions. The experimental CCS of 2382 Å² for the 9+ charge state of the 1:1 complex agrees reasonably well with the calculated CCS of 2290 Å² for the top-scoring AF2 prediction. For $A\beta$ bound to the β LG dimer, we obtained a CCS of 3716 Å² for the 13+ ion, again similar to the expected CCS of 3850 Å² for the highest-scoring complex model. Despite this agreement, it must be kept in mind that CCS data are not specific to each complex architecture. Even structurally dissimilar complexes can have near-identical CCSs. This point becomes clear when comparing the top-scoring models for $A\beta$ bound to β LG, which have the flexible N-terminal segment of $A\beta$, collapsed on the surface of β LG. Such a collapse is likely to occur in the gas phase for all the proposed complex structures (31), meaning any of the proposed complexes will likely have similar CCS values regardless of the placement of the $A\beta$ peptide. In summary, the insights from AF2, native MS, and IM-MS show that β LG captures $A\beta$ monomers through nonspecific interactions that are likely to involve the exposed dimer interface.

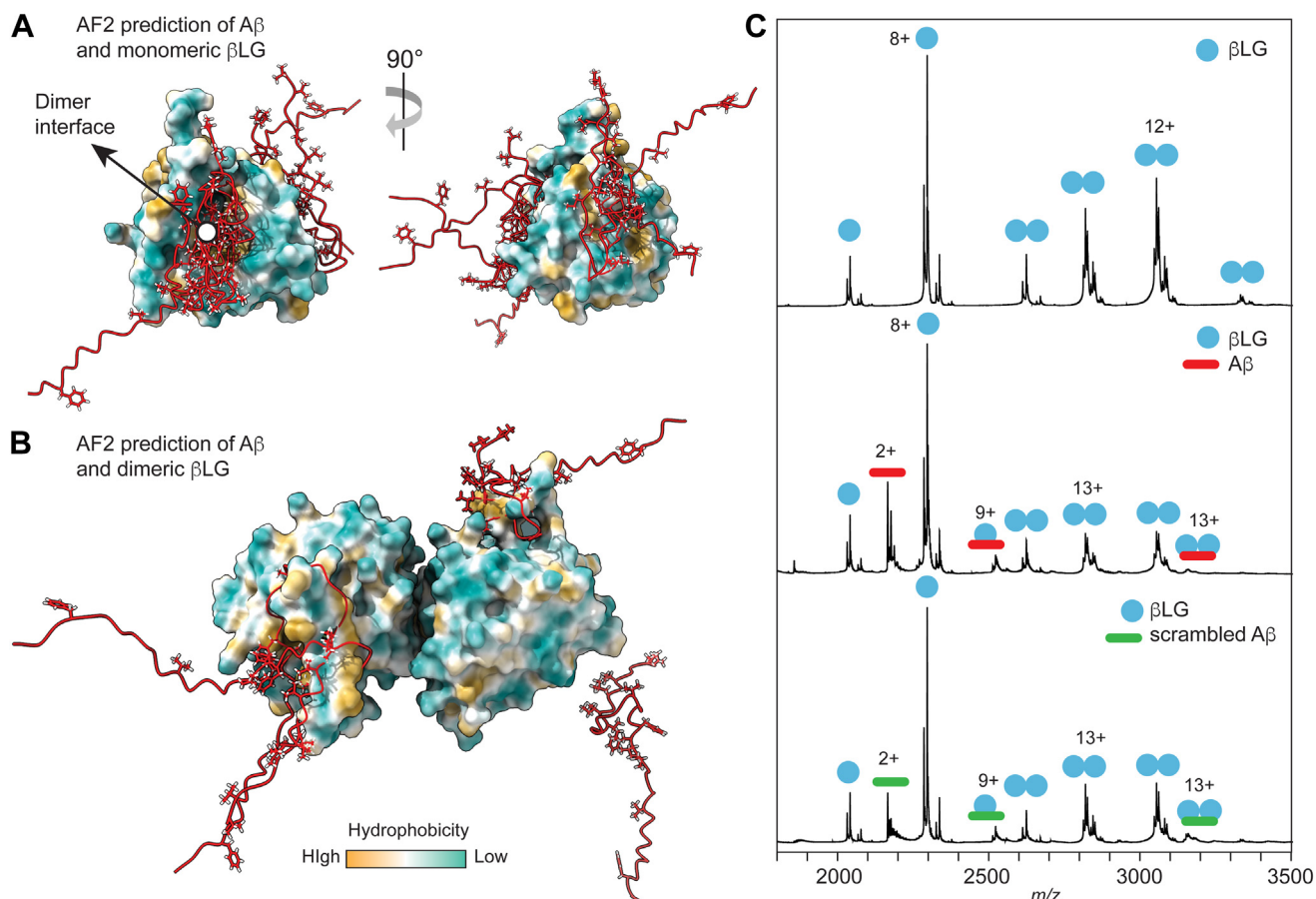


FIG. 1. **Interactions between A β and β LG.** *A*, the overlay of the top five AF2 models of monomeric A β (shown in red with hydrophobic residues rendered as sticks) bound to β LG (rendered as hydrophobicity surfaces) show orientation of hydrophobic residues toward hydrophobic surfaces including the exposed dimer interface. *B*, the top four AF2 predictions of dimeric β LG with A β show random placement of A β on hydrophobic patches of the dimer surface. Coloring as in (*A*). *C*, native MS analysis shows pronounced binding of A β to β LG monomers and a reduced amount of dimers. Replacement of A β with a scrambled A β sequence also results in complex formation. β , amyloid β ; AF2, AlphaFold2; β LG, β -lactoglobulin; MS, mass spectrometry.

It should be noted that nonspecific protein–ligand interactions are a well-known phenomenon in native MS (e.g., (32)). Nonspecific interactions in solution and during electrospray ionization (ESI) are broadly similar, as both are driven by complementary charges, hydrogen bonds, and hydrophobic interactions between ligand and protein. The ESI process can give rise to nonspecific adducts if protein and ligand are present in the same electrospray droplet. The likelihood of this scenario has been estimated to increase at ligand and protein concentrations above 50 μ M (33). Although the concentrations used in this study are lower (supplemental Table S1), we cannot exclude that complex formation between A β and β LG occurs at least in part during ESI.

Binding of Monomeric A β to TTR and T80 Requires Exposed Subunit Interfaces

Having established that AF2 and MS accurately reflect the nonspecific nature of β LG chaperoning, we turned to TTR. It was recently reported that the anti-amyloid activity of TTR is

inversely correlated to the thermodynamic stability of its tetramer state (13), suggesting that binding to exposed hydrophobic surfaces on the dissociated monomer could be of importance. AF2 models of A β with different TTR species indicate binding of A β to hydrophobic patches in TTR monomers and dimers at the dimer–dimer interface (supplemental Fig. S3), in close analogy to what was observed for β LG. The central hydrophobic segment A β (12–28) displayed the most specific binding mode (Figs. 2A and S3), in agreement with modeling in a previous study (16). AF2 modeling of tetrameric TTR in complex with the monomer of this A β segment resulted in a top-scoring model where the A β (12–28) binds in the central hydrophobic channel at the TTR dimer–dimer interface, whereas the other four AF2 models positioned the peptide randomly around the TTR tetramer (Fig. 2B). We next performed native MS to experimentally test these predictions. Weak binding of A β (12–28) to TTR at a 1:4 stoichiometry was observed, with the intensity of the peaks increasing upon overnight incubation at room temperature

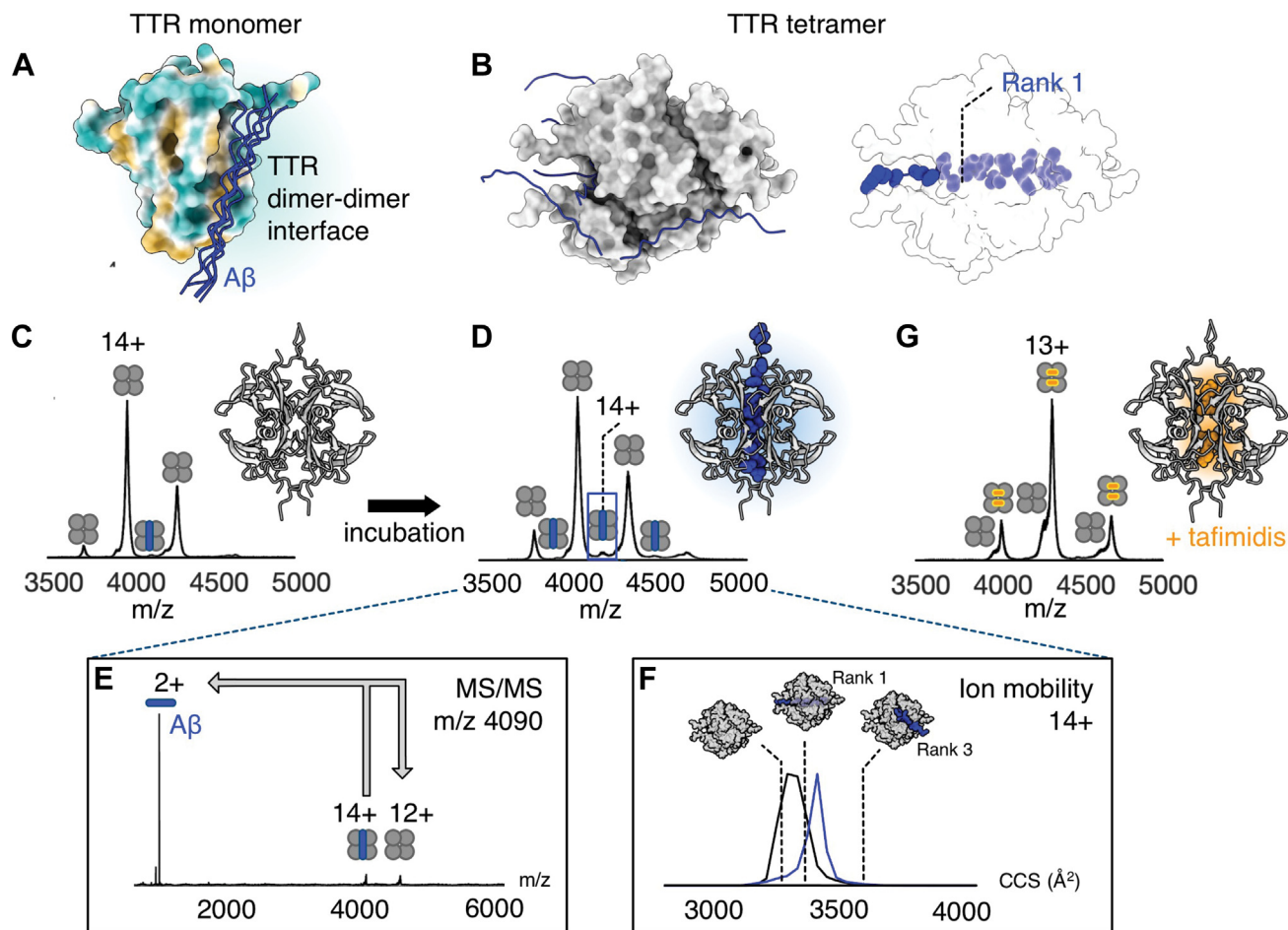


FIG. 2. Interactions between A β and TTR. *A*, AF2 predictions of the A β (12–28) segment interacting with the TTR monomer. The five top-scoring AF2 models are shown in a *blue cartoon* representation, and TTR is shown in a surface representation colored according to hydrophobicity. *B*, AF2 prediction of A β (12–28) binding to the TTR tetramer shows the positioning of the peptide in the central hydrophobic channel (rank 1), far away from the TTR tetramer (rank 2) and close to the surface of the TTR tetramer (ranks 3–5). *C*, native MS spectrum of TTR and A β (12–28) at a 1:1 ratio just after mixing shows a weak signal of a TTR–A β heterocomplex, with TTR shown as *gray circles*, whereas A β is illustrated as a *blue rod*. *D*, signals for TTR–A β heterocomplexes increase in intensity after incubation overnight at room temperature. *E*, the identity of the heterocomplex was confirmed using MS/MS. *F*, ion mobility measurements show that the CCS of the heterocomplex is closer to the AF2 rank 1 structure with A β bound inside the TTR tetramer, rather than the AF2 rank 3 structure with A β bound on the surface of TTR. The arrival time distribution of apo-TTR is shown in *gray*, that of the TTR–A β (12–28) complex in *blue*. *G*, further evidence for binding in the central channel is given by the minimal A β binding to TTR after overnight incubation, when the tetramer is stabilized by coinhibition with tafimidis. A β , amyloid β ; AF2, AlphaFold2; CCS, collision cross-section; TTR, transthyretin.

(Fig. 2, C and D). Complex formation was confirmed using MS/MS (Fig. 2E). To test whether A β could interact with TTR monomers, we turned to the TTR_{F87M,L110M} mutant, which is a constitutive monomer in solution (34). We found that the peptide readily bound to the TTR mutant, in good agreement with previous studies (supplemental Fig. S3) (35). We next employed IM analysis of the A β –TTR 1:4 heterocomplex to compare the calculated CCS values for the predicted models to experimental values. The experimental CCS (3418 Å²) for the 14+ charge state of the 1:4 complex agreed best with the top-scoring prediction by AF2 (3374 Å²), where the peptide is bound in the hydrophobic pocket at the dimer–dimer interface (Fig. 2F). The model with A β bound to the surface of the TTR

tetramer had a significantly larger CCS (3610 Å²) than that observed experimentally. The CCS values do not imply a specific architecture, but since TTR undergoes little compaction in the gas phase (36), the data support the top-scoring AF prediction. Native MS thereby confirms A β monomer binding to the TTR tetramer, and IM measurements enable us to accept or reject predicted complex architectures.

Binding of A β to the hydrophobic pocket is likely dependent on dissociation of the TTR tetramer. The influence of subunit exchange rate on complex formation was tested experimentally by adding the small organic drug molecule tafimidis, which increases the stability of the tetrameric form of TTR (37). In the presence of tafimidis, we observed a clear decrease in

A β binding to TTR (Fig. 2G) after incubation. This finding suggests that the stabilized form of TTR is unable to bind A β peptides, where the hydrophobic patches, suggested by AF2 as favorable binding sites, are inaccessible. In summary, the AF2 predictions and IM-MS experiments support a model where dissociated TTR monomers bind monomeric A β through hydrophobic interactions between the TTR dimer-dimer interface and the central hydrophobic core of A β .

Next, we asked whether a similar mechanism could be observed for T80, which has antiamyloid activity *in vitro* and is implicated in AD. AF2 predictions of monomeric T80 and A β indeed suggest binding to this region (supplemental Fig. S4). Predicting the complex between dimeric T80 and A β yielded a sandwich-type structure in which the A β peptide is located between the T80 protomers. We tested this unusual model with native MS using the same approach as for β LG and TTR. Under native conditions, T80 forms mostly dimers and tetramers, but no binding of A β could be detected (supplemental Fig. S4). However, when T80 and A β were incubated at 95 °C for 30 min prior to MS analysis, we observed increased monomerization of T80 as well as minor adduct peaks corresponding in mass to a 1:1 complex (supplemental Fig. S4). We conclude that in T80 dimers, the hydrophobic patch at the dimer interface is inaccessible to interactions with monomeric A β . We speculate that for T80 to exert an antiamyloid activity, like β LG, A β would be required to encounter T80 monomers, for example, during dimer formation *via* the α -secretase cleavage.

Pro-SP-C BRICHOS Binds Polyvaline Sequences Through β -Strand Trapping

For SP-C and CTC, although a highly specific chaperone-client pair, it is not yet clear whether selectivity is governed solely by the fact that they are synthesized as part of the same polypeptide chain, or whether CTC in addition displays sequence preferences. Recent data support that proSP-C BRICHOS binds its target polyvaline stretch in the transmembrane domain, and the mutations in the proSP-C BRICHOS domain result in incorrect folding of the polyvaline transmembrane region (38). We have previously turned to MS to establish client preferences and interaction sites in CTC, and using native MS and model peptide ligands, we found that CTC preferentially binds to hydrophobic peptides with a high β -strand propensity, with polyvaline displaying the highest relative affinity. Interestingly, peptide binding was observed with CTC monomers even when the crystal structure shows a trimer (19–21). Using HDX-MS, we furthermore found that a polyvaline ligand (KKVVVVVVVKK, termed V7), as well as a VLEM motif (residues 68–71) in the disordered region of CTC, become ordered upon binding, suggesting that V7 and the disordered region form complementary structures (21).

We used AF2 to generate a model of the full-length CTC monomer bound to V7 for comparison to the crystal structure of the proSP-C BRICHOS domain (Fig. 3A). AF2 accurately

predicted both the BRICHOS structure and the disordered loop region between the two helices. The V7 peptide was consistently predicted to bind to a groove formed by the BRICHOS domain and the disordered region that folds back on the BRICHOS domain (Fig. 3A). This specific structural rearrangement is in contrast to the random placement of A β on the surface of β LG (Fig. 1, A and B) and TTR. Alignment of the resulting complex with the trimeric BRICHOS crystal structure shows extensive steric clashes (Fig. 3B).

To test whether V7 binding is indeed incompatible with CTC trimerization, we recorded native MS spectra of CTC in the presence of increasing amounts of V7 (Fig. 3C). In agreement with previous studies (39), CTC formed trimers and monomers as well as a low amount of dimers that we attributed to in-source dissociation of trimers. The amount of CTC trimers decreased below a protein:ligand ratio of 3:1 (Figs. 3C and S5). V7 was found to interact with CTC monomers, although only a small fraction of CTC retained the V7 ligand in the gas phase. We have previously used native MS to determine relative affinities of CTC to model peptides and found that polyvaline exhibited the lowest gas-phase K_d , but underwent significant in-source dissociation (20), providing a possible rationale for this observation. We conclude that V7 likely interacts both with the folded BRICHOS domain and the disordered region in CTC.

For a more detailed view of such a potential interaction, we reconsidered our previous HDX-MS data: in the absence of V7, the VLEM peptide (the central region of the disordered part) is subject to rapid deuterium incorporation, reaching full labeling within 1 min (Fig. 3D) (21). Notably, the VLEM peptide is the only region of CTC where we could detect an interaction with V7 by HDX-MS (supplemental Fig. S6). In the presence of V7, the VLEM peptide displays a maximum labeling of less than 50% (21). Similarly, the V7 ligand becomes nearly fully deuterated in the absence of CTC but exhibits significant protection from labeling when coincubated with CTC (Fig. 3D). In the AF2 model, the VLEM region forms a β -strand that runs antiparallel to the V7 peptide, which in turn binds as an extension to the central β -sheet of the BRICHOS domain. Notably, the side chains of V7 made only sparse contacts with the surrounding residues in CTC.

Together, these data indicate that binding to CTC is mostly driven by the pronounced β -sheet propensity of the ligand. To test this hypothesis, we performed AF2 and HDX-MS analysis of CTC with a helical peptide ligand (KKAAAAAAAKK, termed A7). AF2 models show no binding of A7 to any defined region of CTC with the disordered region in random orientations (supplemental Fig. S7). This result is in good agreement with previous data showing that CTC binds differently, depending on the secondary structure of the substrate peptide (40), and HDX-MS revealed no increased protection of A7 in the presence of CTC. Similarly, the VLEM motif showed complete labeling even upon coincubation with A7 (supplemental Fig. S7).

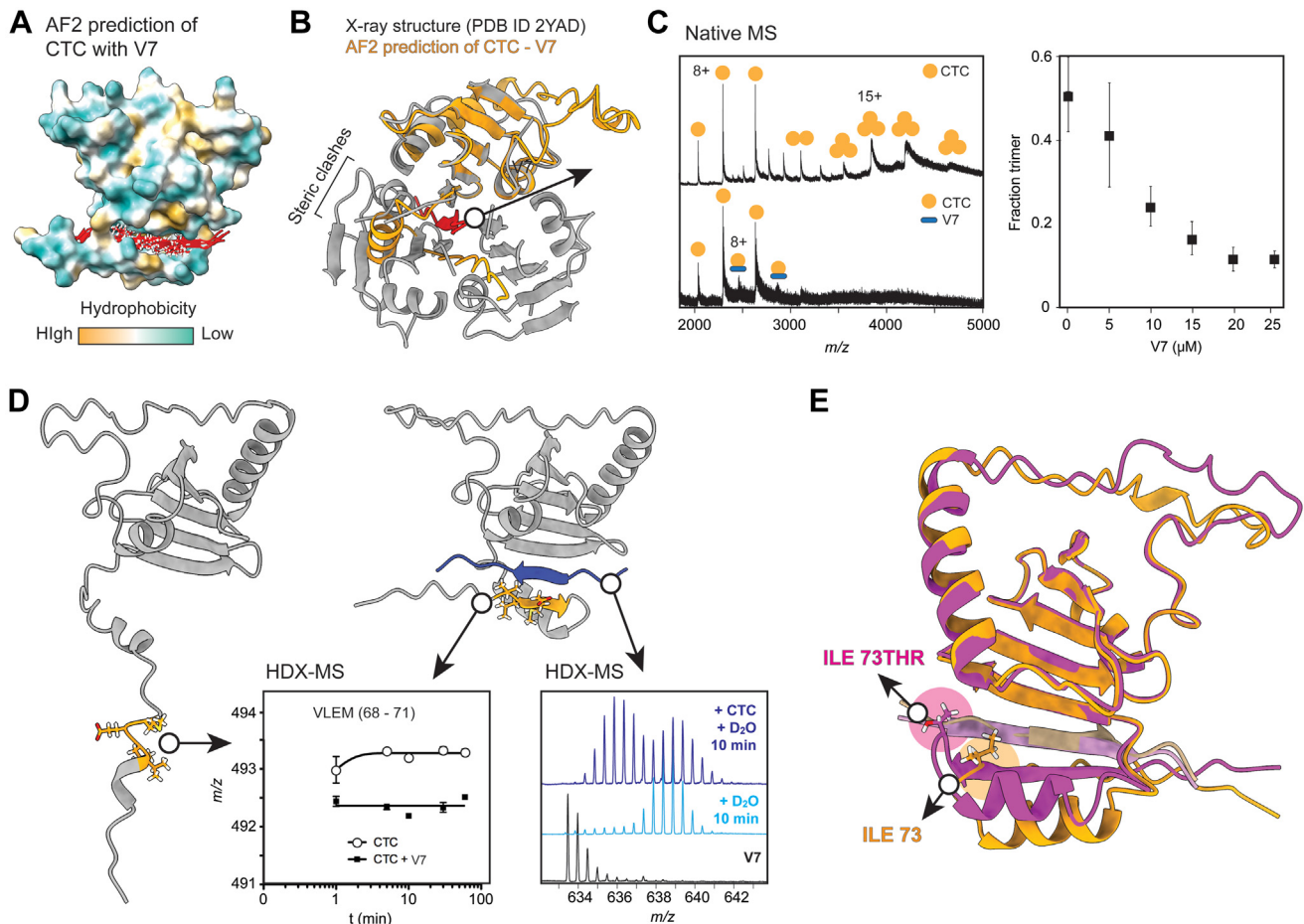


FIG. 3. Recognition of polyvaline by the CTC. A, overlays of the top five CTC-V7 complex predictions show consistent placement of the V7 ligand in a groove formed by the BRICHOS domain and the disordered region. CTC is shown as a hydrophobicity surface rendering and V7 as a *red ribbon* with valine residues as *sticks*. B, overlay of the proSP-C BRICHOS crystal structure (*gray*) with the AF2 model of CTC bound to V7 (*orange* and *red*, respectively) shows clashes between the disordered region of CTC and the BRICHOS trimer. C, native MS of CTC shows binding of V7 to monomeric CTC. Plotting the relative abundances of trimeric CTC in mass spectra recorded at increasing V7 concentrations reveals a trimer-to-monomer transition, with error bars representing the standard deviation from three independent experiments. D, AF2 models of ligand-free CTC (*left*) and CTC bound to V7 (*right*) suggest that V7 and the VLEM motif (residues 66–71 in proSP-C) form complementary β -strands. HDX-MS shows increased protection of both peptides from deuteration upon complex formation. E, overlay of AF2 predictions of wildtype CTC (*orange*) and the I73T mutant, *pink*, showing a loss of the hydrophobic contact between I73 and the polyvaline ligand as well as an upward shift of the disordered region in the mutant. I73 and T73 are shown as *sticks*. AF2, AlphaFold2; CTC, C-terminal region of proSP-C; HDX-MS, hydrogen-deuterium exchange coupled with mass spectrometry; proSP-C, proform of lung surfactant protein C.

The finding that the central part of the disordered region forms a complementary β -strand pair with the polyvaline substrate has an interesting implication: one of the most prevalent genetic defects linked to interstitial lung disease is a missense mutation in proSP-C leading to the replacement of isoleucine 73 with a threonine directly adjacent to the VLEM motif (I73T) (41, 42). Based on the excellent agreement between the AF2 models and the MS data, we decided to delineate the effect of the I73T mutation on ligand binding using AF2 (Fig. 3E). The model shows that the mutation leads to a loss of hydrophobic interactions between isoleucine 73 and the C-terminal valine residue of V7. Instead, T73 appears to hydrogen bond with the ligand backbone, pulling the rest of the disordered region upward. We conclude that the mutation

interferes with the ability of CTC to keep its ligand in an extended conformation, providing a rationale for its effect on pathogenic SP-C misfolding (42).

A high propensity to fold into β -sheet structures is a common property of amyloidogenic peptides/proteins, and the mechanism observed here for CTC/V7 appears to be a general mechanism for anti-amyloid activity in chaperones. A structurally similar example is DNAJB6, a Hsp40-type chaperone that specifically binds amyloidogenic peptides including polyQ peptides and A β (43–45). All Hsp40 chaperones consist of a highly conserved N-terminal J-domain, which recruits Hsp70, and a client binding C-terminal domain, which is specific for the client protein of the chaperone. The C-terminal domain in DNAJB6 forms a single β -sheet that could bind clients with

β -sheet propensity. AF2 modeling of A β and the C-terminal domain of DNAJB6 does indeed predict highly specific binding of A β in a β -hairpin conformation to the edge strand of the chaperone β -sheet (supplemental Fig. S7). This binding site is not a hydrophobic interface, as the edge strand is rich in polar serine and threonine residues known to be of importance for the antiamyloid activity of the chaperone (46, 47). Such specific binding is therefore driven by complementary conformations rather than hydrophobic interactions.

CONCLUSIONS

In this study, we have combined AF2 structure prediction with native MS, IM-MS, and HDX-MS to compare nonspecific interactions with specific chaperone–peptide interactions. AF2 and IM-MS show that the nonspecific chaperone activity of β LG and TTR toward A β is due to hydrophobic interactions between the peptide and the proteins. Access to hydrophobic surfaces can be subject to regulation *via* conformational dynamics. Consequently, very stable assemblies such as T80 and tafamidis-stabilized TTR appear to be poorer binders of amyloid peptides. On the other hand, the specific interaction between the polyvaline region of SP-C and its C-terminal BRICHOS domain is driven by the strong β -strand propensity of the ligand, which is trapped by a complementary β -strand of the disordered region of proSP-C, as shown here by AF2, native MS, and HDX-MS. This binding mechanism is similar to those suggested for other dedicated antiamyloid chaperones, such as the DNAJB6 chaperone. In summary, the combination of machine learning and MS-based structural proteomics now reveals the details of previously inaccessible protein interactions. We anticipate that this methodology, in the future, will allow successful modeling of further relevant protein complexes, such as peptide–drug binding, and hormone–receptor interactions.

DATA AVAILABILITY

The raw IM-MS and HDX-MS data in PULSAR and .txt formats, respectively, are available from the DRYAD repository, <https://doi.org/10.5061/dryad.r2280gbgj>.

Supplemental data—This article contains supplemental data.

Acknowledgments—Computational resources: Swedish National Infrastructure for Computing, grants: SNIC 2021/5-297, SNIC 2021/6-197, and Berzelius-2021-29. Special thanks for technical support is extended to MS Vision, NL.

Author contributions—N. Ö., A. L., A. E., J. J., C. S., and M. L. methodology; N. Ö., A. L., and M. L. investigation; A. G., H. J., L. L. I., and E. G. M. resources; N. Ö., T. V., and M. L. writing—original draft.

Funding and additional information—M. L. is supported by a Karolinska Institutet (KI) faculty-funded career position, a KI-Cancer Blue Sky grant, a Cancerfonden project grant (grant no.: 19 0480), the Olle Engkvist Foundation, and a Swedish Research Council (VR) starting grant (grant no.: 2019-01961). M. L. gratefully acknowledges further financial support from Swedish Research Council grant for internationally recruited scientists (grant no.: 2013-08807) to Prof Sir David Lane, KI. C. S. is supported by a Novo Nordisk Foundation postdoctoral fellowship (grant no.: NNF19OC0055700). L. L. I. is supported by the Swedish Research Council grant no. VR-2021-04744 and the Olle Engkvist Foundation. Native MS instrumentation was supported by a SciLifeLab Technology Development grant to L. L. I. A. E. is supported by Swedish Research Council for Natural Science, grant no. VR-2016-06301, Swedish E-science Research Centre, and the Knut and Alice Wallenberg Foundation. E. G. M. is supported by a Swedish Research Council project grant (grant no.: 2020-04825).

Conflict of interest—The authors declare no competing interests.

Abbreviations—The abbreviations used are: A β , amyloid β ; AD, Alzheimer's disease; AF2, AlphaFold2; β LG, β -lactoglobulin; CCS, cross-section; CTC, C-terminal region of proSP-C; ESI, electrospray ionization; HDX, hydrogen–deuterium exchange; IM, ion mobility; MS, mass spectrometry; proSP-C, proform of lung surfactant protein C; TTR, transthyretin.

Received July 14, 2022, and in revised form, September 8, 2022
Published, MCPRO Papers in Press, September 15, 2022, <https://doi.org/10.1016/j.mcpro.2022.100413>

REFERENCES

- Landreh, M., Sawaya, M. R., Hipp, M. S., Eisenberg, D. S., Wüthrich, K., and Hartl, F. U. (2016) the formation, function and regulation of amyloids: insights from structural biology. *J. Intern. Med.* **280**, 164–176
- Eisenberg, D., and Jucker, M. (2012) The amyloid state of proteins in human diseases. *Cell* **148**, 1188–1203
- Chiti, F., and Dobson, C. M. (2017) Protein misfolding, amyloid formation, and human disease: a summary of progress over the last decade. *Annu. Rev. Biochem.* **86**, 27–68
- Jucker, M., and Walker, L. C. (2013) Self-propagation of pathogenic protein aggregates in neurodegenerative diseases. *Nature* **501**, 45–51
- Greenwald, J., and Riek, R. (2010) Biology of amyloid: structure, function, and regulation. *Structure* **18**, 1244–1260
- Chuang, E., Hori, A. M., Hesketh, C. D., and Shorter, J. (2018) Amyloid assembly and disassembly. *J. Cell Sci.* **131**, jcs189928
- Eisele, Y. S., Monteiro, C., Fearn, C., Encalada, S. E., Wiseman, R. L., Powers, E. T., et al. (2015) Targeting protein aggregation for the treatment of degenerative diseases. *Nat. Rev. Drug Discov.* **14**, 759–780
- Goldschmidt, L., Teng, P. K., Riek, R., and Eisenberg, D. (2010) Identifying the amyloids, proteins capable of forming amyloid-like fibrils. *Proc. Natl. Acad. Sci. U. S. A.* **107**, 3487–3492
- Hochberg, G. K. A., Ecroyd, H., Liu, C., Cox, D., Cascio, D., Sawaya, M. R., et al. (2014) The structured core domain of α B-crystallin can prevent amyloid fibrillation and associated toxicity. *Proc. Natl. Acad. Sci. U. S. A.* **111**, E1562–E1670
- Luo, J., Wärmländer, S. K. T. S., Gräslund, A., and Abrahams, J. P. (2014) Non-chaperone proteins can inhibit aggregation and cytotoxicity of Alzheimer amyloid β peptide. *J. Biol. Chem.* **289**, 27766–27775

11. Landreh, M., Rising, A., Presto, J., Jörnvall, H., and Johansson, J. (2015) Specific chaperones and regulatory domains in control of amyloid formation. *J. Biol. Chem.* **290**, 26430–26436
12. Ghadami, S. A., Chia, S., Ruggeri, F. S., Meisl, G., Bemporad, F., Habchi, J., et al. (2020) Transthyretin inhibits primary and secondary nucleations of amyloid- β peptide aggregation and reduces the toxicity of its oligomers. *Biomacromolecules* **21**, 1112–1125
13. Jayaweera, S. W., Surano, S., Pettersson, N., Oskarsson, E., Lettius, L., Gharibyan, A. L., et al. (2021) Mechanisms of transthyretin inhibition of iapp amyloid formation. *Biomolecules* **11**, 411
14. Du, J., Cho, P. Y., Yang, D. T., and Murphy, R. M. (2012) Identification of beta-amyloid-binding sites on transthyretin. *Protein Eng. Des. Sel.* **25**, 337–345
15. Cho, P. Y., Joshi, G., Johnson, J. A., and Murphy, R. M. (2014) Transthyretin-derived peptides as β -amyloid inhibitors. *ACS Chem. Neurosci.* **5**, 542–551
16. Gimeno, A., Santos, L. M., Alemi, M., Rivas, J., Blasi, D., Cotrina, E. Y., et al. (2017) Insights on the interaction between transthyretin and A β in solution. A saturation transfer difference (STD) NMR analysis of the role of iododiflunisal. *J. Med. Chem.* **60**, 5749–5758
17. Gil-Bea, F., Akterin, S., Persson, T., Mateos, L., Sandebring, A., Avila-Cariño, J., et al. (2012) Thioredoxin-80 is a product of alpha-secretase cleavage that inhibits amyloid-beta aggregation and is decreased in Alzheimer's disease brain. *EMBO Mol. Med.* **4**, 1097–1111
18. Hedlund, J., Johansson, J., and Persson, B. (2009) BRICHOS - a superfamily of multidomain proteins with diverse functions. *BMC Res. Notes* **2**, 180
19. Johansson, H., Eriksson, M., Nordling, K., Presto, J., and Johansson, J. (2009) The Brichos domain of prosurfactant protein C can hold and fold a transmembrane segment. *Protein Sci.* **18**, 1175–1182
20. Fitzen, M., Alvelius, G., Nordling, K., Jörnvall, H., Bergman, T., and Johansson, J. (2009) Peptide-binding specificity of the prosurfactant protein C Brichos domain analyzed by electrospray ionization mass spectrometry. *Rapid Commun. Mass Spectrom.* **23**, 3591–3598
21. Willander, H., Askarieh, G., Landreh, M., Westermarck, P., Nordling, K., Keränen, H., et al. (2012) High-resolution structure of a BRICHOS domain and its implications for anti-amyloid chaperone activity on lung surfactant protein C. *Proc. Natl. Acad. Sci. U. S. A.* **109**, 2325–2329
22. Knight, S. D., Presto, J., Linse, S., and Johansson, J. (2013) The BRICHOS domain, amyloid fibril formation, and their relationship. *Biochemistry* **52**, 7523–7531
23. Jumper, J., Evans, R., Pritzel, A., Green, T., Figurnov, M., Ronneberger, O., et al. (2021) Highly accurate protein structure prediction with AlphaFold. *Nature* **596**, 583–589
24. Baek, M., DiMaio, F., Anishchenko, I., Dauparas, J., Ovchinnikov, S., Lee, G. R., et al. (2021) Accurate prediction of protein structures and interactions using a three-track neural network. *Science* **373**, 6557
25. Tsaban, T., Varga, J. K., Avraham, O., Ben-Aharon, Z., Khramushin, A., and Schueler-Furman, O. (2022) Harnessing protein folding neural networks for peptide-protein docking. *Nat. Commun.* **13**, 176
26. Allison, T. M., Degiacomi, M. T., Marklund, E. G., Jovine, L., Elofsson, A., Benesch, J. L. P., et al. (2022) Complementing machine learning-based structure predictions with native mass spectrometry. *Protein Sci.* **31**, e4333
27. Lössl, P., Waterbeemd, M., and Heck, A. J. (2016) The diverse and expanding role of mass spectrometry in structural and molecular biology. *EMBO J.* **35**, 2634–2657
28. Allison, T. M., Reading, E., Liko, I., Baldwin, A. J., Laganowsky, A., and Robinson, C. V. (2015) Quantifying the stabilizing effects of protein-ligand interactions in the gas phase. *Nat. Commun.* **6**, 8551
29. Marklund, E. G., Degiacomi, M. T., Robinson, C. V., Baldwin, A. J., and Benesch, J. L. P. (2015) Collision cross sections for structural proteomics. *Structure* **23**, 791–799
30. Benesch, J. L. P., and Ruotolo, B. T. (2011) Mass spectrometry: come of age for structural and dynamic biology. *Curr. Opin. Struct. Biol.* **21**, 641–649
31. Rolland, A. D., and Prell, J. S. (2019) Computational insights into compaction of gas-phase protein and protein complex ions in native ion mobility-mass spectrometry. *Trac - Trends Anal. Chem.* **116**, 282–291
32. Kitova, E. N., Soya, N., and Klassen, J. S. (2011) Identifying specific small-molecule interactions using electrospray ionization mass spectrometry. *Anal. Chem.* **83**, 5160–5167
33. Benesch, J. L. P., Ruotolo, B. T., Simmons, D. A., and Robinson, C. V. (2007) Protein complexes in the gas phase: technology for structural genomics and proteomics. *Chem. Rev.* **107**, 3544–3567
34. Jiang, X., Smith, C. S., Petrassi, H. M., Hammarström, P., White, J. T., Sacchetti, J. C., et al. (2001) An engineered transthyretin monomer that is nonamyloidogenic, unless it is partially denatured. *Biochemistry* **40**, 11442–11452
35. Du, J., and Murphy, R. M. (2010) Characterization of the interaction of β -Amyloid with Transthyretin monomers and tetramers. *Biochemistry* **49**, 8276–8289
36. Hall, Z., Politis, A., Bush, M. F., Smith, L. J., and Robinson, C. V. (2012) Charge-state dependent compaction and dissociation of protein complexes: insights from ion mobility and molecular dynamics. *J. Am. Chem. Soc.* **134**, 3429–3438
37. Bulawa, C. E., Connelly, S., Devit, M., Wang, L., Weigel, C., Fleming, J. A., et al. (2012) Tafamidis, a potent and selective transthyretin kinetic stabilizer that inhibits the amyloid cascade. *Proc. Natl. Acad. Sci. U. S. A.* **109**, 9629–9634
38. Pobre-Piza, K. F. R., Mann, M. J., Flory, A. R., and Hendershot, L. M. (2022) Mapping SP-C co-chaperone binding sites reveals molecular consequences of disease-causing mutations on protein maturation. *Nat. Commun.* **13**, 1821
39. Sahin, C., Österlund, N., Leppert, A., Johansson, J., Marklund, E. G., Benesch, J. L. P., et al. (2021) Ion mobility-mass spectrometry shows stepwise protein unfolding under alkaline conditions. *Chem. Commun.* **57**, 1450–1453
40. Johansson, H., Nerelius, C., Nordling, K., and Johansson, J. (2009) Preventing amyloid formation by catching unfolded transmembrane segments. *J. Mol. Biol.* **389**, 227–229
41. Cameron, H. S., Somaschini, M., Carrera, P., Hamvas, A., Whitsett, J. A., Wert, S. E., et al. (2005) A common mutation in the surfactant protein C gene associated with lung disease. *J. Pediatr.* **146**, 370–375
42. Nerelius, C., Martin, E., Peng, S., Gustafsson, M., Nordling, K., Weaver, T., et al. (2008) Mutations linked to interstitial lung disease can abrogate anti-amyloid function of prosurfactant protein C. *Biochem. J.* **416**, 201–209
43. Månsson, C., Kakkar, V., Monsellier, E., Sourigues, Y., Härmärk, J., Kampinga, H. H., et al. (2014) DNAJB6 is a peptide-binding chaperone which can suppress amyloid fibrillation of polyglutamine peptides at sub-stoichiometric molar ratios. *Cell Stress Chaperones* **19**, 227–239
44. Månsson, C., Arosio, P., Hussein, R., Kampinga, H. H., Hashem, R. M., Boelens, W. C., et al. (2014) Interaction of the molecular chaperone DNAJB6 with growing amyloid-beta 42 (A β 42) aggregates leads to sub-stoichiometric inhibition of amyloid formation. *J. Biol. Chem.* **295**, 8135–8144
45. Österlund, N., Lundqvist, M., Ilag, L. L., Gräslund, A., and Emanuelsson, C. (2020) Amyloid- β oligomers are captured by the DNAJB6 chaperone: direct detection of interactions that can prevent primary nucleation. *J. Biol. Chem.* **295**, 8135–8144
46. Karamanos, T. K., Tugarinov, V., and Marius Clore, G. (2020) An S/T motif controls reversible oligomerization of the Hsp40 chaperone DNAJB6b through subtle reorganization of a β sheet backbone. *Proc. Natl. Acad. Sci. U. S. A.* **117**, 30441–30450
47. Månsson, C., van Cruchten, R. T. P., Weininger, U., Yang, X., Cukalevski, R., Arosio, P., et al. (2018) Conserved S/T residues of the human chaperone DNAJB6 are required for effective inhibition of A β 42 amyloid fibril formation. *Biochemistry* **57**, 4891–4892